A SIMPLIFIED LITHIUM VAPOR BOX DIVERTOR

R.J. GOLDSTON
Princeton University / Princeton Plasma Physics Laboratory
Princeton NJ, USA
Email: goldston@pppl.gov

E.D. EMDEE
Princeton University / Princeton Plasma Physics Laboratory
Princeton NJ, USA

M.E. RENSINK
Lawrence Livermore National Laboratory
Livermore CA, USA

T.D. RONGLIEN
Lawrence Livermore National Laboratory
Livermore CA, USA

J.A. SCHWARTZ
Princeton University / Princeton Plasma Physics Laboratory
Princeton NJ, USA

Abstract

A detached divertor is predicted to be necessary to mitigate the heat fluxes and electron temperature, and so sputtering, at the divertor plate of a fusion power plant. The lithium vapor box divertor localizes dense lithium vapor to induce detachment at a stable location. The vapor localization is formed by local evaporation and nearby condensation, in effect strong differential pumping. The paper provides a simulation of lithium vapor flow using the SPARTA Direct Simulation Monte Carlo (DSMC) code. We find that a simplified lithium vapor box configuration, without baffles, provides robust stabilization and minimum lithium vapor flow. Lithium condensed on the side walls of the divertor must flow back down to a porous target "sponge" at the bottom of the divertor. To provide enough lithium vapor to induce full detachment in the Fusion Nuclear Science Facility divertor requires evaporation of 124 g/s of lithium, which is recondensed on the divertor walls at a temperature of order 300 C, and must flow back to the evaporator. If the first wall of the main chamber is maintained at temperature of order 600 C, little lithium will accumulate in the main chamber. A 10 cm wide evaporator is cooled, by net evaporation, at a rate of about 900 kW/m^2, while condensation elsewhere on the chamber walls provides localized heating of about 200 kW/m^2. Radiation from the plasma provides up to 2 MW/m^2 of heating, spread over much of the divertor surface area.

1. INTRODUCTION

An attached divertor is likely to have heat fluxes and electron temperatures too high for a fusion power plant. The lithium vapor box divertor design achieves detachment while localizing the lithium vapor that absorbs the plasma heat flux. The lithium is contained in the divertor region through poloidal baffles creating a series of "boxes". Each box is kept at a separate wall temperature with higher temperatures closer to the divertor target. These boxes cause differential pumping, with net condensation in the box farthest from the target and net evaporation closer to the target. In this way, lithium could be contained to the divertor region while maintaining densities high enough to detach the plasma. Extending this analysis, we explore demonstration of lithium vapor localization and resulting detachment stability in a much simplified configuration without baffles.

2. SPARTA

The Stochastic PArallel Rarefied-gas Time-accurate Analyzer (SPARTA) Direct Simulation Monte-Carlo (DSMC) code was used to analyze lithium behavior in a baffled and unbaffled detached divertor design SPARTA moves particles through a Cartesian grid within a 2D simulation of the vapor box geometry. The grid cells are used to group particles together to determine collision rate.

A Variable Hard Sphere (VHS) model with velocity-dependent effective diameter is employed for neutral-neutral collisions calibrated to lithium vapor's temperature-dependent viscosity. The form for the viscosity is given by [1]

$$10^{-7}\mu = 130.6 + 0.1014 \cdot (T - 1000) - 4.55 \cdot 10^{-6} \cdot (T - 1000)^2$$

Where T is in K and μ in SI units. This form is then matched to T^{ω} over the range of 700K - 1000K and ω is provided as an input parameter to SPARTA.

The walls simulate evaporation and condensation by emitting particles and absorbing all impacting particles. Particle emission is simulated as a half Maxwellian distribution of velocities with the temperature of the wall and the equilibrium density of lithium at that temperature. The equilibrium density is determined by using the pressure curve for lithium given by [1].

$$logP = 13.0719 - \frac{18880.659}{T} - 0.4942 \cdot logT$$

where P is given in MPa and T in K. The SPARTA code was modified with an axial weighting scheme to have a more even distribution of simulation particles. The modified weighting achieved a factor of ~ 10 decrease in processing time for a given statistical accuracy.

3. PLASMA MODEL

Since SPARTA is incapable of modeling charged particles in electromagnetic fields, a simple model is used to determine the effect of plasma absorption on the neutral lithium. In this model, the plasma is treated as a fixed surface, idealizing the ionization front.

Simulations of FNSF [2] with lithium-induced detachment in UEDGE [3] indicate that lithium recombines roughly where it is ionized, as shown in Figure 1. This implies that lithium ionized on a given field line contributes to the lithium density on that field line, but in steady-state is largely recombined on the same field line. This is simulated in SPARTA by assuming that all neutral lithium that crosses the plasma boundary is ionized there, and an equal rate is recombined. Upon recombination the neutral lithium is given both a temperature and a directed energy along $\vec{B}$ of 0.2 eV. The FNSF plasma shape in SPARTA is set by the UEDGE ~ 0.2 eV electron temperature contour, which is a good approximation of the ionization and recombination region in UEDGE.

Note that UEDGE has a different neutral transport model than SPARTA. UEDGE uses a purely diffusive model balancing the gas pressure with the momentum transfer to unlike particles, such as hydrogen ions/gas and lithium ions. This results in a gas velocity of the form

$$V_g = \frac{D}{P_g} \nabla P_g$$

Where

$$D = \frac{T_g}{m_g \nu_{elastic}}$$

and $\nu_{elastic}$ is the elastic collision frequency for neutrals colliding with ions. Note that UEDGE does not take into account neutral-neutral collisions, unlike SPARTA, which does not take into account neutral-ion collisions. Thus, due to the different models in UEDGE and SPARTA, some disagreement between the two simulations is to be expected. Evidently both forms of collision are physically present, but in our recombined scenarios most of the lithium transport occurs in regions where the lithium density is much greater than the plasma density.

For the FNSF simulations, UEDGE indicates there is an average cooling per ionized lithium atom of ϵ_{cool} = 60 eV, and 66 MW of power to be dissipated, consistent with 1.1 MA = 79 g/s of lithium ionization. The cooling per atom is predicted to be larger when the lithium is absorbed on field lines closer to the separatrix due to higher upstream temperatures [4]. Thus, as baffles are added and lithium is more localized, less lithium injection would be required. Accordingly, our prediction of the absolute amount of lithium escaping the baffled region is likely an overestimate for FNSF.

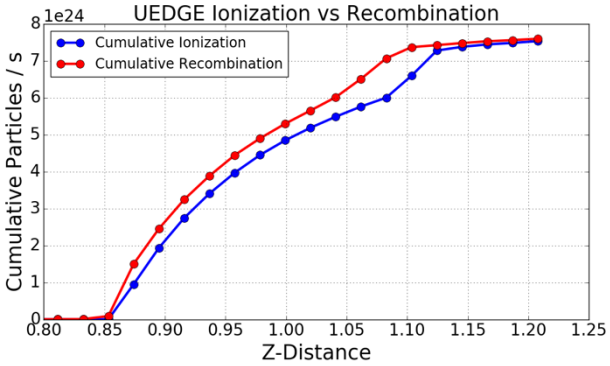

FIG 1: The cumulative ionization and recombination from the target to the Z-position in a UEDGE simulation of lithium injection to the divertor. This indicates that the plasma displaces lithium slightly towards the divertor, but overall effectively acts as a mirror.

4. SIMULATION OF THE FUSION NUCLEAR SCIENCE FACILITY DIVERTOR

We now proceed to add baffles to the SPARTA simulation and change the boundary conditions to be more realistic. The absorbing walls were changed to cold lithium walls with very little evaporation and zero reflection. Furthermore, since there is much less heat delivered on the private-flux side of a divertor leg, it should be easier to detach the divertor leg from that side, and the private flux region (in FNSF) provides a more closely coupled plasma "mirror" for lithium. Accordingly, we choose to evaporate lithium from the private-flux side of this divertor as shown in Figure 2. Comparing to cases with a more diffuse injection region, the private flux injection showed significant improvements to lithium vapor localization.

Due to the small divertor volume in FNSF, only two chambers were employed as opposed to the three chambers in the idealized design given earlier. The top of the 300 C baffles acts a collector of lithium while the warm walls emit lithium at 400 C. The hottest wall temperature is adjusted to give 66 MW of cooling power at ϵ_{cool} = 60 eV. For two baffles, a temperature of 897 C was needed, on the 10 cm – wide evaporating region to create power balance, while the unbaffled case required 742 C. This resulted in lithium injection rates of 17 MA and 1.7 MA for the two baffle case and the unbaffled case respectively. Since both cases were normalized to give ionization rates of 1.1 MA, the unbaffled case will require significantly less lithium recirculation.

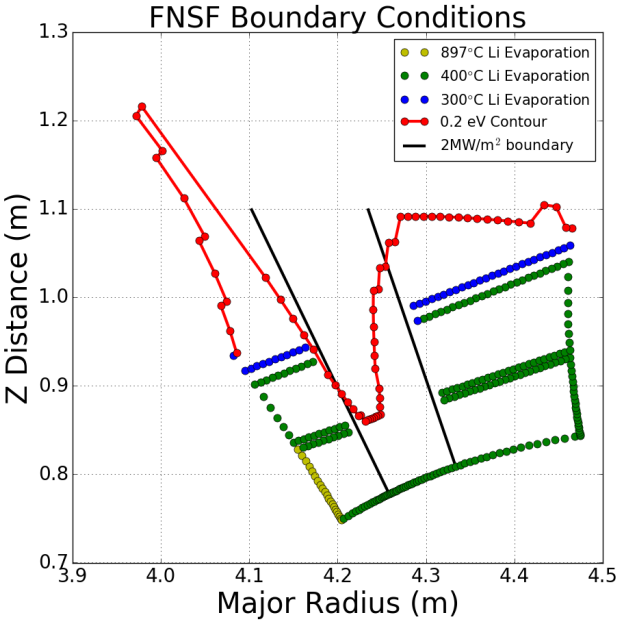

FIG 2. A diagram of the boundary conditions given to the FNSF SPARTA simulation. All neutral lithium crossing the 0.2 eV contour is re-emitted at the same location. To increase localization, all lithium was emitted only from the private-flux side.

A comparison of the different baffling is given in Figure 3. We see that the addition of the baffles greatly reduces the lithium density outside of the chambers, once again showing the efficacy of differential pumping at reducing the lithium efflux from the baffled region. We quantify this by noting the single baffle configuration had 94.1% of the lithium ionization occurring in the divertor leg, while the case without baffles had 60.1% of the lithium ionizing in the same region. Thus, the addition of baffles to this geometry reduced the far SOL ionization by nearly a factor of eight. Since the main chamber wall in a fusion system is likely to be a temperature in the range of 600 C, it will function as, essentially, a reflecting boundary condition, with little lithium accumulation. This is how it is treated in UEDGE. By considering the case with no baffles, we are allowing this outer SOL ionization.

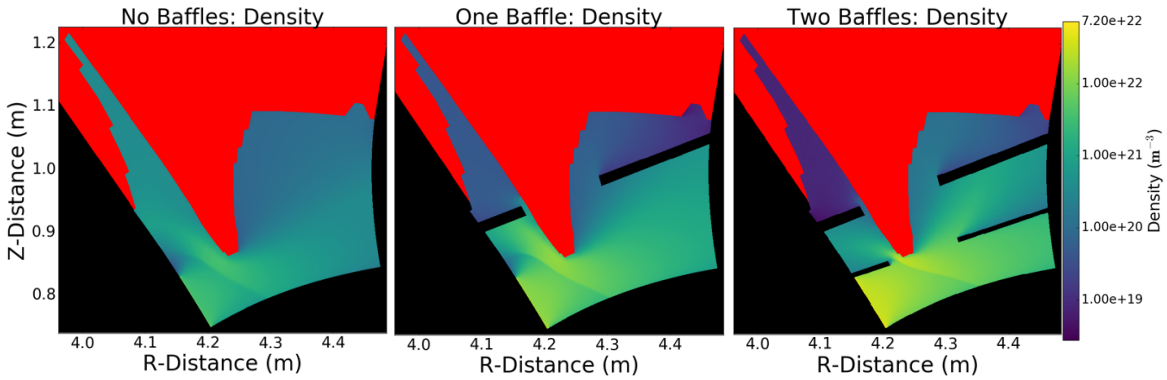

FIG 3: A plot of lithium vapor density in FNSF with no baffles, one baffle, and two baffles with private-flux side lithium evaporation. We see here that the density outside the baffled region is greatly reduced by the presence of baffles, showing localization of lithium to the divertor leg.

4.1. VAPOR BOX RESILIENCE TO POWER CHANGES

The addition of the second baffle provided only a modest increase to 94.9% of the lithium ionization in the leg. The benefit to localization of the second set of baffles seems insignificant in this unoptimized geometry where the apertures are similar in width to the box height. However, the double baffle design is shown to be more resilient to changes in plasma heating power. In Figure 4 we adjust the detachment position in the previous simulations over a range of 19 cm, and hold the wall temperatures constant. From this we can estimate the effect of increased power on the detachment front position. The amount of lithium ionized on the divertor leg in the double baffle case increases by a factor of 18 between 13 cm farther from the target to 6 cm closer to the target. This is a significant improvement over the case without the baffles, which underwent a factor of six change in ionization at the divertor leg. We note, however, that a factor of six variation should still provide for strong stabilization of the divertor leg location.

With further optimization, e.g a more closed divertor geometry, the unbaffled configuration may provide more position resilience. Resilience to Edge Localized Modes, which cause rapid increases in heat flux to the divertor plate would be a major advantage for this configuration. If enough lithium were provided in a bottom "sponge" the immediate heat flux of the thermal quench of disruptions could be handled as well. The heat of vaporization of lithium is about 10 MJ/liter, and one would expect significant vapor shielding. A 10 cm deep sponge, containing 50% lithium, with width of 10 cm, would contain 132 liters. For both ELMs and disruption thermal quenches, the more open geometry of the no-baffle case might be more effective at capturing the transient heat flux, which is spread more widely than in quiescent operation.

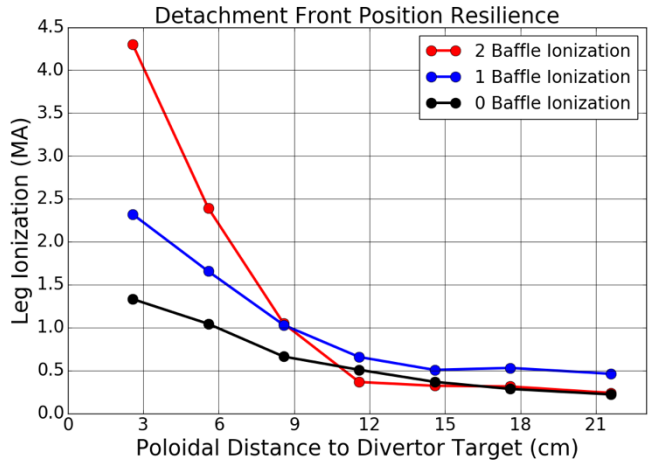

FIG 4: A plot of the divertor leg ionization using the wall temperatures determined for the plots in Figure 3, but with different distances from the detachment front to the divertor target.

5. LITHIUM FLOWS AND THERMAL EFFECTS

We have evaluated the implied flows of lithium, as shown in fig. 5. The lithium mass flow has a typical value of 40 g/s, extending over a typical poloidal distance of 30 cm. If we choose to drive this flow back to the emitting source by capillary force alone, we can estimate the flow speed following the analysis of [5] for a single wick. This gives

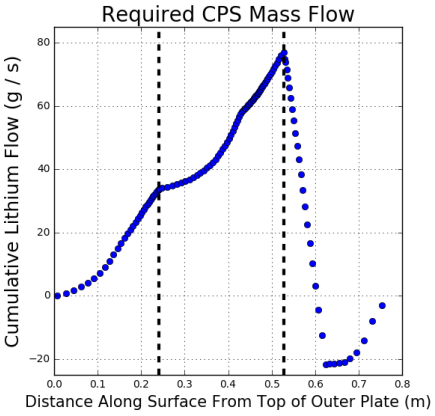

$$Q = \frac{A}{L}\frac{2\gamma cos\alpha / r_w}{3\mu / r_w^2 + \sigma B^2}$$

We use the parameters in [5] for lithium surface tension, γ, wetting angle, α, kinematic viscosity, μ, and thermal conductivity, σ, at 600 K. If we take the pore size to be 10 μm, the magnetic field to be 7 T, and the connection length to 0.3 m, we find that a capillary porous material depth of 6 mm would be required. This is sufficiently thick that it should removed behind the path of the surface heat flux to the coolant. Evidently this is a more convenient flow rate that that required for the multi-baffle cases.

FIG 5. Poloidal lithium flow to replenish evaporation in no-baffle case.

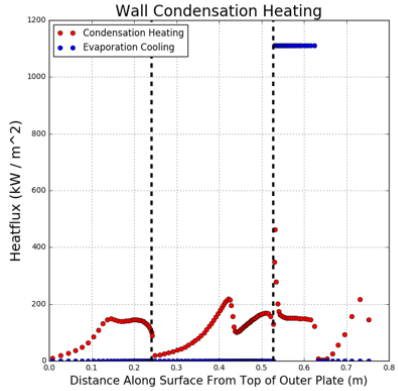

We have also calculated the local cooling and heating rate from evaporation and condensation, shown in Fig. 6. We find that the peak local net cooling, of about 900 kW/m^2 is less than the heating by radiative losses of about 2 MW/m^2, so it will not be necessary to provide heating to this surface during long-pulse operation. Elsewhere the heating due to condensation is small compared to radiative heating.

FIG 6. Poloidal lithium flow to replenish evaporation in no-baffle case.

6. CONCLUSIONS

We have found that a lithium vapor box without baffles provides much of the advantages of a heavily baffled configuration, with the exception that more lithium flows into the far SOL region of the plasma. Since the first wall in a fusion power system will operate at a temperature in the range of 600 C where we do not expect lithium condensation, this may not be an overwhelming advantage. The simpler configuration still provides strong localization of the lithium vapor and so the detachment front, and has additional robustness against ELMs and even disruption thermal quenches. This geometry would also be easier to test in near-term experiments, including initial configurations with only a toroidal segment installed.

ACKNOWLEDGEMENTS

This work is sponsored under DOE Contracts No. DE-AC02-09CH11466 and DE-AC52-07NA27344.

REFERENCES

[1] OHSE, R.W, Handbook of Thermodynamic and Transport properties of Alkali metals (1985) Blackwell Scientific Publications, 350

[2] KESSEL, C.E. et al., The Fusion Nuclear Science Facility, the critical step in the pathway to fusion energy, Fusion Science and Technology, Fusion Science and Technology 68:2 (2015) 225-236, DOI: 10.13182/FST14-953

[3] ROGNLIEN, T.E. et al., Simulations of a high-density, highly-radiating lithium divertor, submitted for publication to Nuclear Materials and Energy (2018)

[4] GOLDSTON, R.J. et al., Recent advances towards a lithium vapor box divertor, Nuclear Materials and Energy (2017), DOI: 10.1016/j.nme.2017.03.020

[5] RINDT, P., et al., Conceptual design of a pre-loaded lithium divertor target for NSTX-U, Fusion Engineering and Design, 112 (2016) 204